Single Photon Interference

Jaewon Jung[1]

[1] *Department of Physics and Astronomy, Seoul National University, Seoul 08858 Korea*

(Received 31 March 2024; revised 1 April 2024; accepted 3 April 2024; published 4 April)

When the coherent single photon is indistinguishable, it can self-interfere in principle of quantum mechanics. We first show that the diffraction theory holds for waves using the coherent laser source and explore the single photon-limit using the flux-tunable bulb. Considering the line broadening and the asymmetries of slits, we reached the accuracy of 99.9 % in single slit diffraction and double slit interference fringes as well proving that the diffraction theory is valid for waves. We then reached close to the single photon-limit and validated this limit by uncertainty principle and the Poisson distributions of observed signals with 60 Hz noise filtering.

I. INTRODUCTION

In this report, we reproduce the famous Young's double slit experiment using two different light sources, the coherent 670 nm laser and the filtered 546 nm bulb that can be dimmed to the single-photon limit. In comparing the results of the wave-like laser and the particle-like bulb, we explore and verify the wave-particle duality of light. Moreover, we analyze the diffraction and interference patterns considering the line broadening of the two light sources and the limit of Fraunhofer's diffraction theory by introducing the path integral formulation. In particular, we propose a precise and efficient calibration routine for choosing the high-voltage and the threshold value of the Pulse Counter/Interval Timer (PCIT1).

A. Feynman's path integral formulation

In the path integral formulation, a probability amplitude is defined by the complex superposition of all possible trajectories as follows [ref]:

$$K(\beta;\alpha) = \sum_{all\ paths\ \alpha\to\beta} const \cdot e^{i\varphi_{path}}\,, \qquad (1)$$

where all possible paths which connect events α, β. The phase summed along for each path is defined as

$$\varphi_{path} = \frac{1}{\hbar}\int_{path} L(x,\dot{x},t)dt\,, \qquad (2)$$

where L is the Lagrangian and the x, t are the position and time. For the double slit interference experiment, the path difference is simply written as

$$\Delta\varphi = \frac{2\pi}{\lambda}\Delta s, \qquad (3)$$

where s represents the displacement along the corresponding path. Specifically, for the case of TWS2-A device, the intensity at the position (z) in the screen is derived as

$$I(x,z) = \left|\int_{y\in S} e^{\frac{2\pi i}{\lambda}s_1(x,y)} e^{\frac{2\pi i}{\lambda}s_2(y,z)}\right|^2, \qquad (4)$$

where $s_1(x,y) = \sqrt{D_1^2 + (x-y)^2}$, $s_2(y,z) = \sqrt{(D_2+D_3)^2 + (y-z)^2}$ and the corresponding parameters are depicted in FIG. 1. The presence of the blocker slit is ignored in this calculation. The integration domain of path S is the combination of the paths from source slit (P) to detector slit (R) and the additional path integral over *(x-a/2, x+a/2)* and *(z-a/2, z+a/2)* is needed to obtain averaged intensity at the position *z* in the screen.

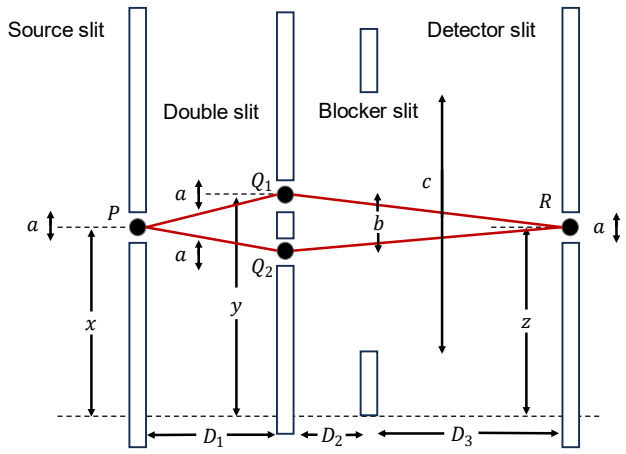

FIG. 1. Paths and locations of each slit of the TSW2-A device for the calculation in path integral. *a*, *c* are the widths of each slit and *b* is the spacing of double slit. $\boldsymbol{D_i}$ is the distance between slits.

B. Fraunhofer diffraction

Under a far-field approximation, the Kirchoff's diffraction formula is simplified to the Fraunhofer diffraction formula. In the Fraunhofer formula, the incident light source that passes the slit is effectively a plane wave that has linearly varying phase across the aperture. In contrast, under a near-field approximation, the Fresnel diffraction theory is needed which accounts for the relative phase of the waves. In the case of two diffraction formulas are not applicable, the path integral formulation described in section A becomes necessary.

The diffraction and interference patterns of the single, double and asymmetric double slits are simply described by Fraunhofer's theory as below

$$I_{single} = \frac{I_0}{4}\left(\frac{sin\beta_0}{\beta_0}\right)^2,$$

$$I_{double} = I_0\left(\frac{sin\beta_0}{\beta_0}\right)^2 \cos^2\gamma,$$

$$I_{asymm} = I_1\left(\frac{sin\beta_1}{\beta_1}\right)^2 + I_2\left(\frac{sin\beta_2}{\beta_2}\right)^2 + 2\sqrt{I_1 I_2}\frac{sin\beta_1 sin\beta_2}{\beta_1\beta_2}\cos(2\gamma+\phi),$$

$$\beta_i = \frac{1}{2}ka_i sin\theta, \qquad \gamma = \frac{1}{2}kbsin\theta, \qquad (5)$$

where, I_0 is central maximum intensity of double slit case and a, b are the width and the spacing for each slit as shown in FIG. 2.

For the double slit case, visibility V and the following mutual coherence [ref] is defined as

$$V = \frac{I_{max} - I_{min}}{I_{max} + I_{min}} = \frac{2\sqrt{I_1 I_2}}{I_1 + I_2}|\gamma_{12}|, \qquad (6)$$

where, γ_{12} is mutual coherence or a normalized coherence function and the other notations have the usual meaning. Assuming the same intensity at each slit in the double slit, visibility reduces to coherence term only which indicates that the visibility can be directly interpreted as the coherence between two light that pass the double slit. This coherence term is a spatial coherence which ranges from 0 to 1, where 1 for fully spatially coherent and the 0 for fully incoherent. For the temporal coherence, which measures the correlation of pair of light from the light source, is defined up to a constant factor by

$$L_c = t_c c \sim \frac{\lambda^2}{\Delta\lambda}, \qquad (7)$$

where, L_c (t_c) is coherence length (time) and n is refractive index of the medium. λ is an average wavelength and $\Delta\lambda$ is a full width at half maximum. The coherence time means that the time needed for the correlation to drops to 0. Therefore, light path should be shorter than the coherence length unless it will lead to speckle kinds of noise. In the Young's double slit experiment, spatial coherence determines the possibility of interference occurrence while temporal coherence is used in the Michelson interferometer.

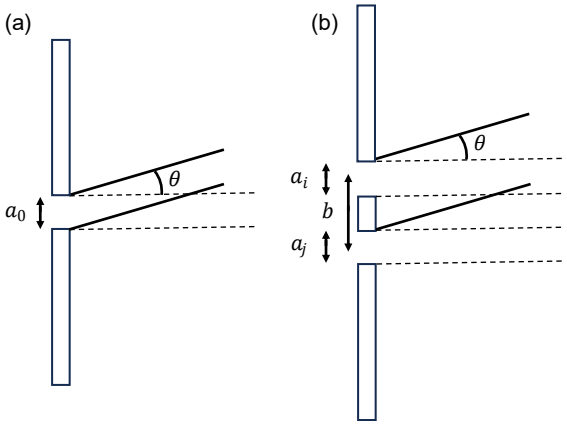

FIG. 2. Diagram of single slit (a) and double slit (b) with the width $\boldsymbol{a_i}$ and the spacing b.

C. Line broadening

When using a real light source such as a laser or bulb, the wavelength of it is not a single defined value. It has its own linewidth which in general can be obtained from Voigt integral [ref] that represents a mixture of both homogeneous and inhomogeneous broadening. Voigt integral is defined as a convolution of a Lorentz distribution and a Gaussian distribution as follows

$$V(x;\sigma,\gamma) = \int_{-\infty}^{\infty} G(x';\sigma)L(x-x';\gamma)dx', \qquad (8)$$

where, $G(x;\sigma)$ is a Gaussian distribution and $L(x;\gamma)$ is a Lorentz distribution, both are normalized and centered to zero and the x represents the shift from it. From the Voigt integral, it is possible to calculate the full width at half maximum (FWHM) of the linewidth. If we consider this distribution, the Eq. 5 is re-defined as below

$$I(\theta) = \int I(\theta,\lambda)\,V(\lambda;\sigma,\gamma)d\lambda, \qquad (9)$$

where, $I(\theta)$ denotes intensity profile in Eq.5.

To understand distinctive contributions of these distributions, it is intuitive to break the Voigt integral

into homogeneous and inhomogeneous part. The Gaussian part comes from the inhomogeneity of the Doppler broadening due to the Maxell-Boltzmann distribution of the velocities of the particles. On the other hand, the Lorentzian part comes from the homogeneity from various sources such as natural spontaneous emission, stimulated emission due to the consequence of a power broadening or a collisional broadening which results in phase shifts in ensemble average due to the elastic collisions ignoring the rare inelastic collisions which can de-excite the atoms.

D. Photon counting

In the regime of a single photon to order of several thousands of photons per second, a photodiode is not capable of detecting these extremely low signals. Instead, owing to a photoelectric effect and the secondary emission, the photomultiplier tubes (PMT) serve as fundamental tool for accurate counting of extremely low currents.

Photoelectric effect is a phenomenon where the electrons are emitted from the work function of metal due to the incident light. The rate at which the electrons are emitted by the incident photons is defined as quantum efficiency due to the probabilistic nature of the process.

Secondary emission is a phenomenon where the primary emitted particles induce the secondary particles to be emitted when they hit the metal surface with sufficient energy.

Putting together those two principles, the PMT is invented and the basic principle is as follows. In the PMT, there are initial cathode and the consecutive dynodes. When the incident photons hit the cathode, primary photoelectrons are emitted and they are accelerated by appropriate voltage applied, therefore, emitted electrons now have enough energy to hit the following dynodes and start to trigger a chain reaction of the secondary emissions from successive dynodes. As a result, incident small signals from photons are converted to massive currents which is easily detectable. Since the secondary emitted electrons don't go straight to the next dynodes, collection efficiency is also defined due to the deviations in trajectories of emitted electrons.

II. METHODS

In this experimental setup, we employ the TeachSpin's Two-Slit Apparatus with the 1 m optical path [ref] as the base kit for investigating the diffraction and interference phenomena. The detailed set up is shown in FIG. 3. For the light source, 1 mW laser with 670 ± 20 nm and the power-tunable bulb with 546 nm with full width at half maximum (FWHM) of 10 nm which is filtered by the optical filter are used. Single slits are used as a source and detector slit and the three different kinds of double slits are used. The width of single slit and double slit is given by 85 μm. The spacing of double slits are given by 356 μm, 406 μm, 457 μm labeled by no. 14, 15, 16 respectively and the width of blocker slit is measured as 1.778 mm. The distances from each slit are described in the FIG. 3. For the measurement, the photomultiplier tube (PMT) R212 from Hamamatsu, the preamplifer-discriminator Amptek A-111 which has 0.8 %/V threshold coefficient, UNI-T UT802 multimeter and the Pulse counter / Interval timer from TeachSpin are used with the external power supply of 50 ~ 60 Hz.

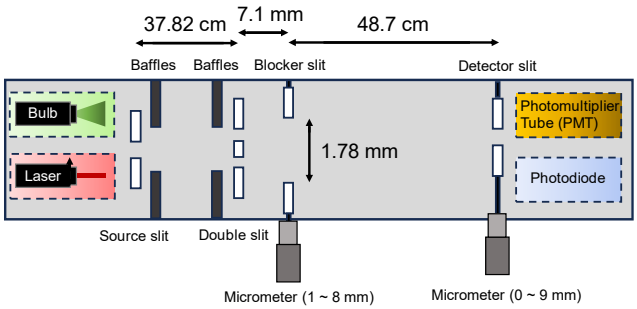

FIG. 3. Configuration of the U-channel from the TWS2-A apparatus.

A. Alignment of U-channel

The main purposes of alignment are (1) to align a source slit to be well-centered to obtain the central peak of diffraction, interference pattern at the center of screen and (2) to align a detector slit well so that the intensity at the center position of the detector slit is well peaked and (3) to align the double slit to be well-centered to obtain the same peak height of the interference fringe to achieve high visibility which is closely related to coherence and (4) to obtain the position profile of blocker slit for the single slit and asymmetric double slit experiment. The alignment procedure for the U-channel is as below.

0) Always double check that shutter is closed and the bulb switch is off to protect the PMT from radiated by strong light.

1) Fix the position of laser tightly to keep the laser aligned throughout out the whole experiment by adjusting the knob and the geometric direction of the laser source by checking if the light from the laser goes straight to the end of the U-channel.

2) Insert the source slit and the detector slit well until the central maxima is centered and narrow enough.
3) Insert the double slit well until the interference fringe is symmetric and well centered.
4) For the final step, insert the blocker slit and the no.14 double slit and record the measured voltage by a photodiode by moving the blocker slit from 1 to 8 mm with 0.05 mm interval using the micrometer in aware of the backlash.

The voltage measurement for the blocker slit is done using the oscilloscope with sampling rate 1 kHz and the 20 MHz bandwidth filter.

A. Diffraction and interference: Laser

For the no. 14, 15, 16 double slits, we conduct the double slit interference experiment for the natural double slit and the asymmetric double slit using the blocker slit. For the single slit experiment, using the blocker position profile, conduct the single slit diffraction experiment for each single slit of no. 14 double slit.

To measure the voltage of photodiode accurately, the MDO 3024 oscilloscope is employed which is capable of setting the 20 MHz bandwidth filter and the time averaging over up to 10 M samples. In balancing the trade-off between accuracy and efficiency, we choose 1000 samples over 1 s. The voltage per each blocker position is measured when the voltage is fully stabilized after each micrometer move.

B. Diffraction and interference: Bulb

For the bulb experiment, extra calibration routine is needed to choose optimal high-voltage applied to photomultiplier tube (PMT) and threshold value for pulse counter/interval timer (PCIT). To optimize this daunting task, we developed efficient and accurate calibration routine that can maximize the signal-to-noise ratio (SNR). The procedure is as below.

1) Find the lower bound and the upper bound of high voltage by measuring the photon count when the shutter is opened and a bulb is on with low intensity or shutter is off respectively.
2) From the high voltage value between the lower bound and the upper bound range to higher high voltage, measure the raw signal output from PMT both when the bulb is turned on and the shutter is off to acquire signal counts and dark counts. In this acquiring stage, 10 M samples with sampling rate 50 MHz for 5 times each are measured using the oscilloscope.
3) Calculate the SNR for each high voltage as varying the threshold value digitally in the local computer.
4) Choose the optimal high voltage and threshold that maximize SNR.
5) Double check if the high voltage and threshold value gives correct photon counts by comparing the output signal of PCIT with the raw signal utilizing the trigger function in the oscilloscope.

High voltage is measured using the multimeter and the output signal of PCIT is measured using the oscilloscope with same setting as the raw signal measurement.

Using the high voltage and threshold obtained from above calibration, we first measure the intensity at each detector position to align the detector slit. Then, we measure the light intensity for each bulb intensity setting the detector at the center position and regress the data to obtain the relation between the light intensity and the bulb intensity.

Now, for the no.14 double slit, we conduct double slit experiment and single slit experiment. Especially, the double slit experiment is conducted as varying the bulb intensity to reach the single-photon limit.

III. RESULTS

A. The intensity profile of a blocker slit

The intensity profile is obtained with an order of 1 mV standard deviation and the steps in intensity are well observed. However, as seen in FIG. 4. The two mid-steps have different heights approximately 760 mV and 920 mV respectively which indicates that the no.14 double slit has slightly different slit widths.

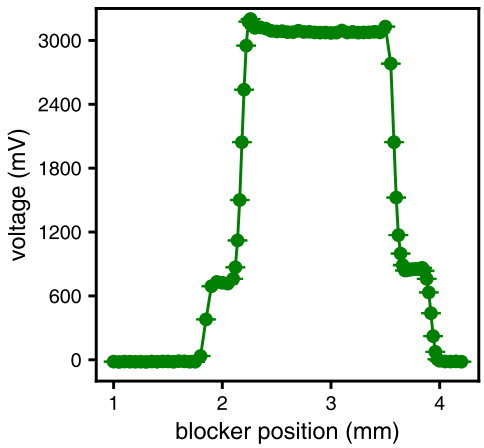

FIG. 4. Measured mean voltage versus blocker position for no.14 double slit.

A. Laser: the double and single slit

The diffraction and interference patterns are well observed as seen in FIG. 5 though there exist non-zero local minimum in the double slit experiments due to the line broadening and asymmetry in the double slit. This is more prominent in no. 16 double slit compared to the other ones leading to poor regression result. The regressions here are done using Eq. 5 without considering the broadening effect. Notably, as observed in the blocker experiment, the intensity of each slit in the no.14 double slit is clearly different. The 1st order visibilities of double slit are 0.909 ± 0.290, 0.955 ± 0.298 and 0.852 ± 0.400 respectively and the corresponding spatial coherence of the no.14 slit is 0.913 ± 0.291. All of uncertainties are calculated using the error propagation technique.

The one sample t-test results are except for the no.14 slit, p-values are above 0.05 that null hypothesis, the slit widths are the same, cannot be rejected within the 5% significance level where p-value of no.14 case is slight below 0.05.

From the asymmetry double slit result, it is observed that peak symmetries are broken due to the different intensity passes through each slit.

Using the Eqs. (8)-(9), the convolution fit results for each double slit are listed in Table I. Using the FWHM obtained, the coherence lengths of each double slit are around 20 μm which is a lot shorter than the optical length which is in an order of meters. But still the interference fringes are well observed since the spatial coherence dominates in the double slit experiment which is high enough to create interference as calculated.

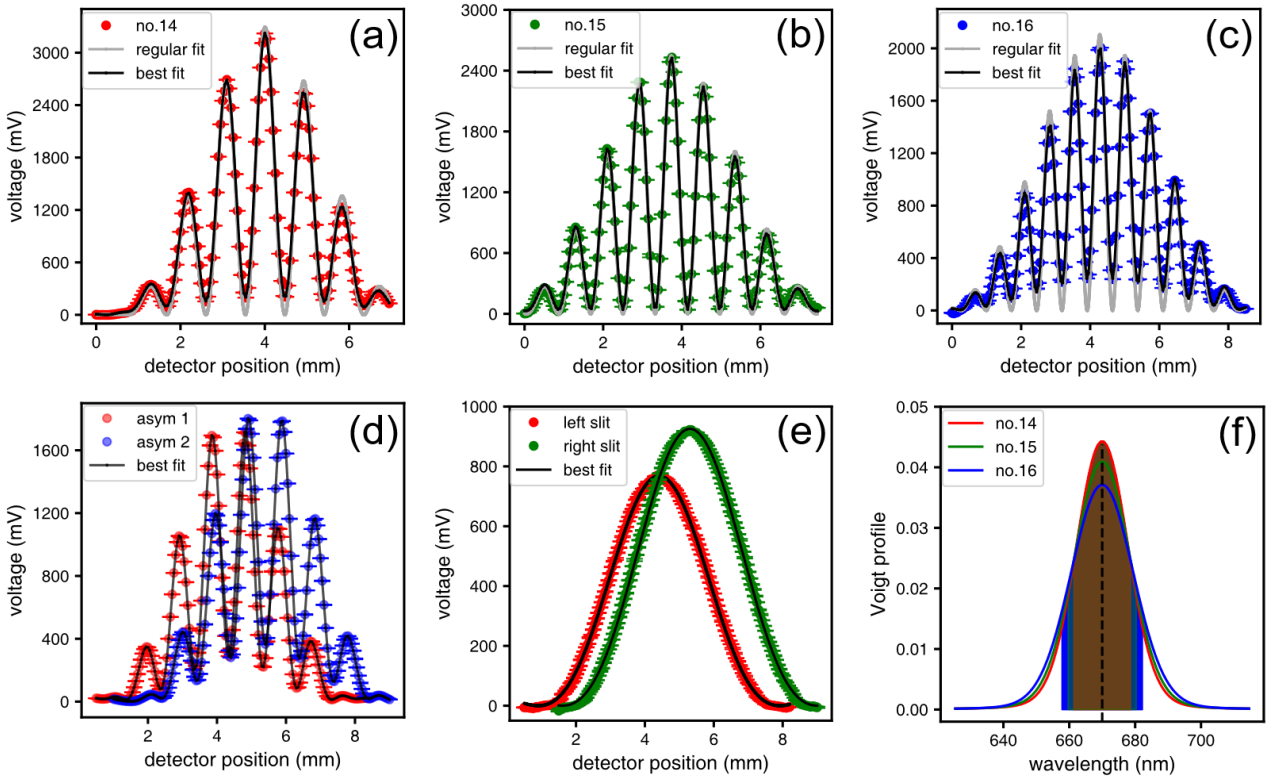

FIG. 5. The diffraction and interference result from the double slit and single slit experiment done by laser. $\boldsymbol{R^2}$ values for each result of without(with) the asymmetry and linewidth are 0.990 (0.9997), 0.997(0.9991), 0.974(0.9997) from (a) to (c) and 0.993, 0.993 for asymmetric 1 and 2 (d) as the same. $\boldsymbol{R^2}$ in (e) are 0.999, 0.999 for left and right slit. (a)-(c) Regular fit means a regression fit without considering asymmetry and linewidth while the best fit considers the both. The filled areas in (f) are the areas where the wavelengths are in the range of FWHM.

TABLE I. The ratio of the widths and p-values from one sample t-test, σ, γ of Voigt integral and full width at half maximum (FWHM) obtained from numerical regressions on the three different double slit results.

Slit	Width ratio	P-value	Spacing ($\boldsymbol{\mu}$m)	$\boldsymbol{\sigma}$ ($\boldsymbol{\mu}$m)	$\boldsymbol{\gamma}$ ($\boldsymbol{\mu}$m)	FWHM (nm)
No.14	1.144±0.012	0.039	348.6±0.015	7.49×10^{-3}	8.36×10^{-4}	18.63
No.15	1.199±0.025	0.078	397.2±0.021	$8.17\times \mathbf{10^{-3}}$	$8.96\times \mathbf{10^{-4}}$	20.23
No.16	1.077±0.059	0.695	446.0±0.009	$9.10\times \mathbf{10^{-3}}$	$8.68\times \mathbf{10^{-4}}$	22.39

B. High voltage and threshold calibration

Utilizing our proposed calibration routine, the optimal high voltage and the threshold value are obtained within 5 minutes. Compared to traditional calibration routine which typically involves using PCIT and manually varying the threshold value, we reduced the total integration time as 10 ~ 20 times faster. In addition, we achieved a significant enhancement in signal-to-noise ratio (SNR) ensured by acquisition of over 10 M data points and post processing. Since the SNR is maximum at high voltage at 540 V and threshold at 1.2 mV, high voltage and threshold value as 540 V and 0 mV are chosen. Setting the threshold of pulse counter (PCIT) doesn't directly mean that the PCIT counts all of the signal because the preamplifier-discriminator adapted in photomultiplier tube helps the counter to eliminate ripple noise and the observed ripple is about 1 mV. SNR in FIG. 6. is calculated by dividing the signal counts by the dark counts.

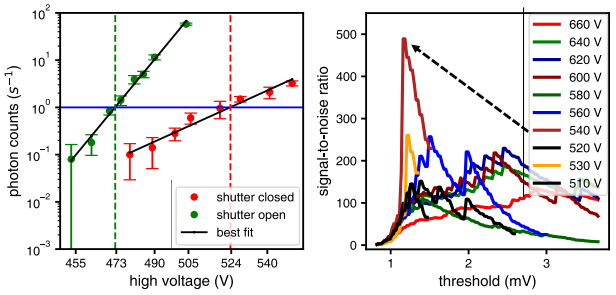

FIG. 6. The log scale result of upper and lower bound calibration (left) and the SNR versus threshold over various high voltages. (right) Linear regression in the log scale is done to find lower and the upper boundaries of high voltage.

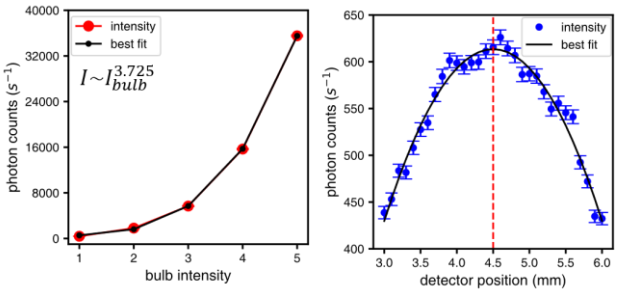

FIG. 7. The photon counts versus bulb intensity and corresponding regression fit. (left) The calibration result of the detector position and the fitted quadrature. (right)

After all the calibration is done, we checked if the designated high voltage and threshold gives the consistent result between raw signal and the PCIT's output as in FIG. 8.

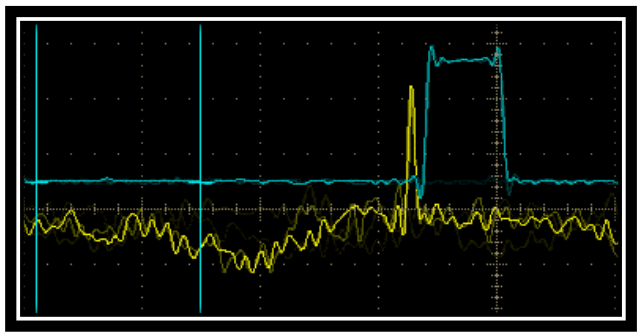

FIG. 8. The screenshot of the oscilloscope for consistency checking between raw signal (yellow) and the PCIT's signal (blue).

C. Bulb: single slit and double slit

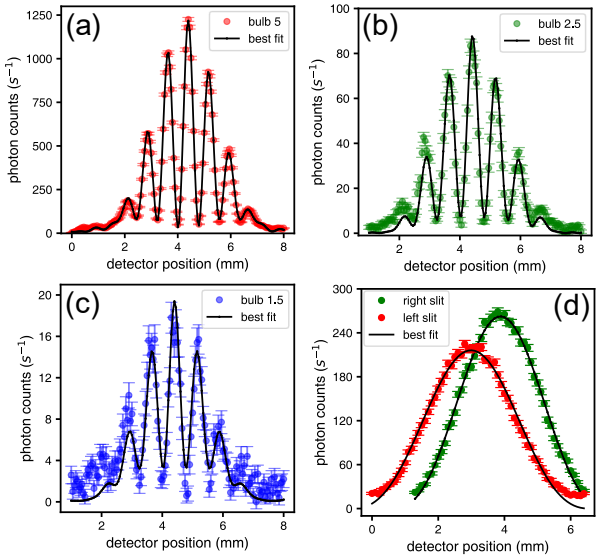

FIG. 9. The double and single slit experiment on the no.14 double slit. (a)-(c) $\boldsymbol{R^2}$ values are 0.999, 0.969 and 0.883 respectively. (d) $\boldsymbol{R^2}$ values are 0.990 (left) and 0.996 (right). Full width at half maximum (FWHM) of (a)-(c) from regression results are 13.45 nm, 4.92 nm and 4.26 nm respectively.

The standard deviations are calculated by square root of the total counts divide by the number of measurements due to the Poisson nature of the photon counting events. All the results are the signal counts where we substitute the dark counts. From the FIG. 9, the maximum photon counts for each slit of the no.14 double slit are 224.9 and 268.9 per second under bulb intensity 5 respectively. Using the photon counts of bulb intensity 5 without double slit in the FIG. 7, photon counts reduce an order of 170 times when it passes the single slit or 680 times when it passes the double slit. The quantum efficiency of R212 PMT with 9 stage we use is around 3 % considering its spectral range and the 546 nm light we use. The collimating lens' efficiency about 70% and assuming

50% collection efficiency, the total efficiency is approximately 1 % which means that photon counts of 200 above is detected from 20000 incident photons. Therefore, an order of 10^4 photons have passed the each slit in the single slit experiment and reduced to several hundreds of photons. Its statistical uncertainty is square root of the total photon counts which are several dozens of photons.

For the double slit experiment, the bulb intensity went down from 5 to 1.5 to achieve the single-photon limit and the result is shown in FIG. 10. The linewidth of the bulb is calculated by the visibility according to the Eq. 10 as below.

$$V = 1 - \left(m\frac{\Delta\lambda}{\lambda}\right), \qquad (10)$$

where, V denotes mth order visibility of double slit interference pattern and note that this equation holds for small angle diffrence. The visibilities measured are 0.935 ± 0.005, 0.928 ± 0.003, 0.922 ± 0.002 for bulb intensity 1.5, 2.5 and 5 and corresponding linewidths are 35.61 ± 2.7 nm, 39.36 ± 1.6 nm and 42.62 ± 1.1 nm.

IV. DISCUSSIONS

A. Misalignment and blocker slit diffraction

In this optics experiment, the most of the errors come from misalignment. On the other hand, there is also a special source that can induce errors on fitting the diffraction pattern due to the presence of blocker slit and the general assumption of far-field can induce rrors as well. But since the blocker slit's width is wide enough that double slit fringes do not get interrupted. Still, we can go further and adopt the Feynman's path integral formulation to see the limit of far-field assumption in our experimental regime. The numerically calculated interference fringes varying the width of blocker slit are shown in FIG. 10.

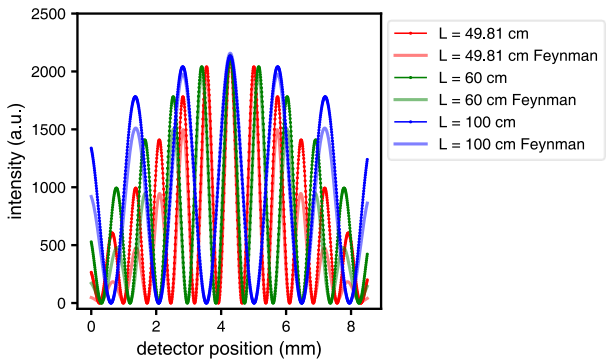

FIG. 10. Double slit interference fringes compared to Fraunhofer (dot) and the Feynman's theory.

As the distance from double slit to detector slit L gets longer, the interference fringes show deviations that we can infer that far-field approximation fails in our distance regime.

B. Voigt profile: Homogeneous and inhomogeneous broadening

In considering the line broadening, two major sources are classified as homogeneous and inhomogeneous broadening. In our experimental setup, laser is coherent, monochromatic source and the bulb is incoherent but filtered that it has finite range of wavelength. Generally, line broadening occurs differently for these two different light sources. For the laser source, the Lorentzian distribution is narrower than the Gaussian distribution and for the bulb, it has broad Gaussian which is filtered that now got narrower and broad Lorentzian distribution. Note that in the room temperature with air, thermal velocity is around 400 to 500 m/s that doppler broadening contribution which results in Gaussian distribution is relatively small. When calculated, the linewidth of the doppler broadening is approximately 0.1 to 0.2 nm. In contrast, Lorentzian part comes mostly from the power broadening in our setting, where the intensity of laser is 1 mW and 10^{-9} to 10^{-6} mW for the bulb. Therefore, we cannot safely say which light source has wider linewidth not knowing the exact saturation intensity to calculate the Lorentzian linewidth. It can be further verified if the power of laser source is adjustable. For the bulb source, using the linewidth for each bulb intensity, the linewidth increases as $\left(1 + \frac{I_0}{I_{saturation}}\right)^{0.875}$ that it is in between homogeneous and inhomogeneous broadening. Notably, the linewidths measured in the bulb experiment doesn't show consistency in fitted result and the ones obtained from visibility. It is concluded that due to the dark rate which obscure the minimum intensity leading to poor calculation of linewidth.

C. 60 Hz noise and noise floor estimation

We use 50~60 Hz power supply which can potentially affect the counting of photons especially when we are measuring very small currents such as the one coming from single photon. As we observe the raw signal as seen in FIG. 10, we can clearly see that there is 60 Hz noise. After applying the Butterworth filter which is capable of passing the wanted frequency signal straight while filter out the unwanted frequencies, we can now see the ripples only signal. The height of this ripples may vary

according to the previous filtering, it is an order of 0.1 mV that we can conclude our thresholding choice is safe from those kinds of ripples. The dark rates are then measured using these filtered signals which are about 4 to 5 counts per second.

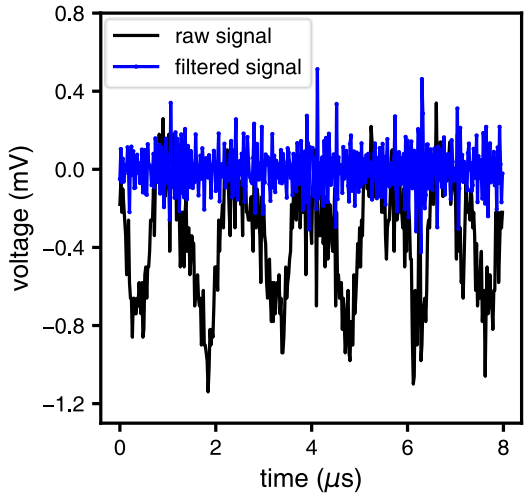

FIG. 11. 60 Hz noise from dark count raw signal and the filtered signal.

D. Verification of single photon limit

As we dimmed the bulb down to bulb intensity 1.5 to achieve single photon-limit and obtained interference fringes, it is necessary to verify if this is result from a single photon or multi-photons regime. R212 photomultiplier tube (PMT) we use has 9 stages of amplifying the initial photoelectrons and secondary emitted electrons, initial single electron is amplified up to 3×10^5 electrons using the multiplication factor of 4. The corresponding currents about 20 μA considering the time interval taken for electrons to arrive is 20 ns. This current passed to 50 Ω resistor then converted to 1 mV and again amplified 20 times before it goes out from the PMT to the pulse counter. Therefore, it is measured around dozens of mV which can vary for the choice of high voltage. Now that for single and multi-photons, they contribute to the signal height differently and it results to roughly a Poisson distribution. As we draw histograms of probability versus pulse height, the result is obvious that as we are lowering the bulb intensity, the peak goes close to zero which is the single photon limit. In the other way, we can calculate the uncertainty relation of position x and momentum p using the linewidth ~ 5 nm obtained from the previous result. $\Delta p = \frac{h}{\lambda^2}\Delta\lambda$, then $\Delta x \sim \frac{\lambda^2}{4\pi\Delta\lambda} \sim$ 5.94±0.12 μm. In the bulb intensity 1.5, using the maximum photon counts around 20, the reducing factor of slit and the 2~3 ns time interval for photons, in the U-channel around 2×10^{-6} photons. Therefore, it can be concluded that the interference fringe in FIG. 9(c). is very much from single photon's self-interference. Also, the bulb is incoherent source that it generally produces less accurate interference fringes. But as it is dimmed to single photon-limit, the visibility goes higher and thus coherence gets bigger as calculated from results section which indicates that the incoherent bulb goes to coherent regime as it goes to single photon-limit.

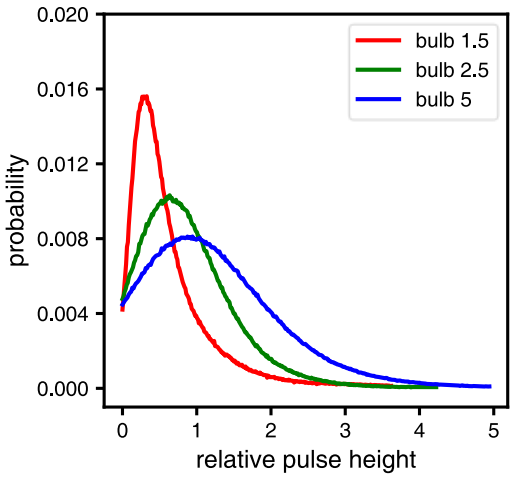

FIG. 12. Poisson distributions from different bulb intensity.

V. CONCLUSIONS

Here, we reproduced the Young's double slit experiment both using the coherent laser source and incoherent but that can be coherent when dimmed to single photon-limit. In the laser experiment, the diffraction theory is verified that the fit results using the Fraunhofer theory with linewidth and asymmetry correction exceed 99.99 % accuracy. In the bulb experiment, we first propose and implemented efficient protocol to calibrate the essential parameters when it comes to photon counting, high voltage and threshold. We then observed interference fringes from the double slit experiment in the single photon regime and this regime is verified by uncertainty principle and the Poisson-like distributions under filtering the 60 Hz noise.

ACKNOWLEDGEMENTS

The author wants to specifically thank our teammates, Juwon Choi, Hyeonsung Jo, Junyoung Lee for conducting the experiments and having

valuable discussions and special thanks to Ysun Choi who provided valuable report to all of us. The author also wants to thank T.A. Keun-Yeol Park for supporting the setup and maintenance of the TWS2-A apparatus, especially the fragile photomultiplier tube.

REFERENCES

[1] Teach spin, TWS2A, Instruction Manual, Rev. 2.0, (2013).
[2] *Photomultiplier Tubes: Basics and Applications (Second Edition)*, Hamamatsu Photonics, Hamamatsu City, Japan, (1999).
[3] R. P. Feynman, R. B. Leighton, and M. Sands, The Feynman Lectures on Physics, vol. I, ch. 37, or vol. III, ch. 1 (Addison-Wesley, 1965).
[4] Mandel, Leonard, and Emil Wolf. "Coherence properties of optical fields." *Reviews of modern physics* 37.2 (1965): 231.
[5] An, Kyungwon. *Fundamentals of Laser Physics*. 2023.